Title	MR study of postnatal development of myocardial structure and left ventricular function
Author(s)	Wu, Y; Wu, EX
Citation	Journal Of Magnetic Resonance Imaging, 2009, v. 30 n. 1, p. 47-53
Issued Date	2009
URL	http://hdl.handle.net/10722/58733
Rights	Creative Commons: Attribution 3.0 Hong Kong License

Original Research

MR Study of Postnatal Development of Myocardial Structure and Left Ventricular Function

Yin Wu, PhD,[1–3] and Ed X. Wu, PhD[1,2]*

Purpose: To investigate postnatal development of left ventricular (LV) cardiac function and myocardium structure.

Materials and Methods: In vivo cardiac MR and ex vivo diffusion tensor imaging (DTI) were performed in normal Sprague-Dawley rats at postnatal day 2, 4, 7, 14, 21, 28, and 56 (N = 6 per group).

Results: Morphologically, LV size increased with age. Functionally, stroke volume and cardiac output increased. Heart rate increased gradually and became stable after day 14. On average, ejection fraction increased within the first 4 days, decreased at day 7, gradually increased until day 21, and became stable afterward. Structurally, double-helical myocardial structure was found as early as day 2. Myocardial fiber parameters, described by fractional anisotropy, mean apparent diffusion coefficient, and axial diffusivity, increased within the first 4 days. Then radial diffusivity increased until day 7 while other parameters decreased up to day 56.

Conclusion: Postnatal heart development was documented by MRI. DTI findings are in agreement with the two known stages of early postnatal growth: hyperplasia and hypertrophy. These results can serve as the baselines for study of postnatal heart developmental abnormalities. They also demonstrate the ability of DTI to reveal microstructural alterations in myocardium.

Key Words: postnatal heart development; cardiac function; myocardium structure; DTI; heart; rat
J. Magn. Reson. Imaging 2009;30:47–53.

GROWTH OF THE HEART is closely coupled with hemodynamic function (1) and important for the growth of all organs (2). The study of concomitant development of cardiac function and myocardium structure cannot only delineate the time course of cardiac maturation, but also provide essential baselines for diagnosis and analysis of cardiac diseases. Rat models have been widely used to assess cardiac functional and structural maturation due to their short development period (3) and relatively large body size to handle.

Functionally, the heart weight has been shown to increase with age (4). The heart rate increases early after birth and then remains relatively constant into adulthood (5,6). During postnatal rat heart development, the heart contractility augments during normal growth in parallel with increase in cell numbers, mitochondrial mass, and myofibrillar ATPase activity (7). The systolic blood pressure doubles from neonate to young adult, and reaches adult levels by 10 weeks of age (8,9). Left ventricle (LV) muscle reaches its functional maturity by postnatal day 16 as assessed by isometric length–tension and pressure–volume time courses in isolated perfused rat hearts (3).

Structurally, two prevailing cellular processes during early postnatal heart growth have been identified using the myocyte isolation and histological techniques: hyperplasia and hypertrophy (5,10–12). Both are capable of responding to the concomitant development of cardiac function, such as increased pressure and volume loads (12). During the first 3–4 days after birth, the volume of myocyte has been shown to remain the same. However, cell number increases, indicating hyperplasia as the dominant factor for heart mass increase (13). Subsequently, myocardial cells lose the dividing capability (14) and the volume begins to increase, then the cardiac enlargement is mainly dominated by myocyte hypertrophy (13). Therefore, a rapid switch from myocyte hyperplasia to hypertrophy occurs around day 4 after birth (13). Similar phenomenon has been observed in mice (15).

Composed of myocytes, myocardial fiber plays a key role in determining LV mechanical properties and electromechanical activations (16–19). Recently, MR diffusion tensor imaging (DTI) has emerged as a powerful tool for rapid measurement of the structure of myocardium (20–25) and skeletal muscle (26) with high spatial resolution nondestructively. Along the myocardial fiber, water diffusion is the greatest, and therefore the primary eigenvector of the diffusion tensor coincides with

[1]Laboratory of Biomedical Imaging and Signal Processing, The University of Hong Kong, Hong Kong, China.
[2]Department of Electrical and Electronic Engineering, The University of Hong Kong, Hong Kong, China.
[3]Institute of Biomedical and Health Engineering, Shenzhen Institute of Advanced Technology, Chinese Academy of Sciences, China.
Contract grant sponsor: Hong Kong Research Grant Council; Contract grant number: GRF HKU 7794/07M.
*Address reprint requests to: E.X.W., Laboratory of Biomedical Imaging and Signal Processing, Department of Electrical & Electronic Engineering, Departments of Medicine and Anatomy, The University of Hong Kong, Hong Kong. E-mail: ewu@eee.hku.hk
Received August 18, 2008; Accepted April 13, 2009.
DOI 10.1002/jmri.21814
Published online 22 May 2009 in Wiley InterScience (www.interscience.wiley.com).

the local fiber orientation. Several studies have characterized myocardial fiber orientation and validated such DTI approach with histological analyses (21,27,28). When viewed from apex, the orientation of LV fibers changes smoothly from a left-handed helix in epicardium to a right-handed helix in endocardium (20–22,27,28). In addition, DTI can assess myocardium structure with quantitative parameters such as fractional anisotropy (FA) and apparent diffusion coefficient (ADC). FA is a normalized scalar measure of the degree of diffusion anisotropy within a voxel and reflects the fiber organization, directional coherence, or integrity. ADC can detect the overall change of water diffusion environment on the cellular level. Using DTI, myocardium structure has been found to degrade in the myocardial infarct as well as the borderzone (29–33). Therefore, DTI analysis may provide insights into the myocardial structural maturation on the microscopic levels during both normal and pathologic development.

In this study, the postnatal cardiac morphological and functional development was investigated in normal Sprague-Dawley (SD) rats using in vivo cardiac MR (CMR) imaging. Concurrently, myocardium structure was investigated using ex vivo DTI. To our knowledge, this is the first study that documents the postnatal development of heart functions and structures using quantitative imaging techniques.

MATERIALS AND METHODS

All MR experiments in this study were conducted on a Bruker 7 Tesla (T) PharmaScan (Bruker BioSpin). All animal experiments were approved by the local institutional ethics committee for animal research.

In Vivo CMR Imaging

CMR imaging of SD rats was examined at 2, 4, 7, 14, 21, 28, 56 days after birth. Around 8 rats were bred per litter before they were weaned at 21 days of age. Six SD rats (N = 6) were used for each time point. Rats were first weighted and then anesthetized with isoflurane for MRI experiments. In this study, 0.5% isoflurane in volume mixed with air was used for rats at age of 2 and 4 days, 0.7% for 7 days, 1.0% for 14 and 21 days, and 1.5% for 28 and 56 days. During MRI, animals were covered with blanket to maintain their physiological body temperature. Electrocardiogram (ECG) electrodes were attached to the front paws and the animals were placed prone over a respiratory sensor. Both ECG- and respiratory-triggering was used during the entire in vivo CMR experiments. To measure LV function, FLASH cine sequence was used to obtain four short-axis slices covering the whole heart (34). The sequence parameters were as follows: TR = 1 R-R interval, TE = 2.3 ms, cardiac frames = 12, matrix size = 192 × 192, flip angle = 30°. In-plane pixel size and slice thickness were heart size dependent and in ranges of 97 × 97 μm^2 ~ 128 × 128 μm^2 and 0.6 ~ 1.6 mm, respectively. The slice gap was set to 10% of slice thickness.

Ex Vivo DTI Study

After in vivo CMR imaging, animals were killed immediately. The hearts were arrested mostly at end diastole and fixed with formalin for 24 h at a room temperature (~20°C). A multi-slice spin echo diffusion tensor imaging (SE-DTI) was performed to acquire short-axis diffusion weighted images at room temperature. Imaging parameters were: repetition time/echo time (TR/TE) = 1500/29 ms, field of view (FOV) = 2.55 × 2.55 cm^2, slice number = 3, b value = 1000 s/mm^2, matrix size = 256 × 256, diffusion gradient duration = 3 ms, diffusion gradient separation = 20 ms, diffusion direction number = 6, and number of averages = 10. Slice thickness was heart size dependent and in the range of 0.6 ~ 1.6 mm with slice gap of 20% of slice thickness. Total image acquisition time was ~7 h per sample.

Data Analysis

In vivo cine images were analyzed for ejection fraction (EF) values using Segment v1.45 software (http://segment.heiberg.se). Endocardium and epicardium contours were semi-automatically defined. End-diastolic volume (EDV) and end-systolic volume (ESV) were measured from the cine image set. Stroke volume (SV) was defined as (EDV-ESV), cardiac output (CO) as (SV × heart rate), and LV EF values as ([EDV-ESV]/EDV). From the end-diastolic images at short-axis view, least-square circle fitting was performed on epicardium on each slice to obtain the epicardium radius for each short-axis slice, among which the largest one was regarded as LV radius.

For ex vivo DTI data, DTI parameters (i.e., FA, mean ADC, eigenvalues, and eigenvectors) were computed from diffusion weighted images (DWIs) using the DtiStudio v2.4 software (Johns Hopkins University; USA) (35). Axial diffusivity was calculated as the primary eigenvalue, that is, parallel to fiber direction. Radial diffusivity was computed as the average of the secondary and tertiary eigenvalues, thus perpendicular to the fiber direction. FA, ADC, and axial and radial diffusivities were computed pixel by pixel within the entire slice with papillary muscles excluded, and averaged among the three short-axis slices for each sample. These DTI parameters were then averaged among six samples of the same age. A MATLAB (MathWorks, Natick, MA) program was developed to compute the fiber helix angle from the primary eigenvector as defined by Chen et al (29) and Scollan et al (21). Helix angle map was generated pixel by pixel for each slice.

One-way analysis of variance (ANOVA) with post hoc Bonferroni's multiple comparison tests were performed on the values describing cardiac morphology, function and myocardium structure for all age groups. Results were considered significant when $P < 0.05$. Unless otherwise stated, all data are presented as means ± standard deviation (SD).

Histological Analysis

After ex vivo DTI study, histological analysis was performed in one of the samples at each age using hematoxylin and eosin (H&E) stain for visualization of myocardium structure. The fixed heart samples were sectioned into 5-μm slices at short-axis orientation. They were then stained with the H&E. Rectangular

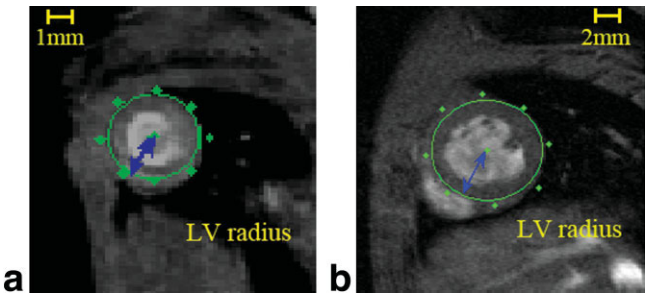

Figure 1. Short-axis view of rat hearts at end-diastole at age of (**a**) postnatal day 2 and (**b**) day 28. Least-squares circle fitting performed on epicardium at the short-axis image, from which LV center was defined and the radius of epicardium was measured. [Color figure can be viewed in the online issue, which is available at www.interscience.wiley.com.]

pieces of myocardium at mid-wall with fibers circumferentially oriented were selected and visualized at ×400 magnification.

RESULTS

Figure 1 illustrates the least-square circle fitting performed on epicardium at a short-axis middle ventricular slice at end-diastole in postnatal day 2 rats (Fig. 1a) and day 28 (Fig. 1b). Heart morphological and functional changes with age are shown in Figure 2. Body weight and LV radius increased dramatically with age (Fig. 2a,b). Heart rate increased significantly from day 2 to day 14, and became steady from day 14 onward (Fig. 2c). On average, EF increased significantly from day 2 to day 4, decreased at day 7, then gradually increased until day 21 (Fig. 2d). Average SV and CO increased significantly with age (Fig. 2e). They mainly responded to the overall mechanical workload as indicated by the strong and positive correlations of SV and CO with body weight and LV radius (Table 1). However, no strong correlations of heart rate and EF with body weight and LV radius were observed. Table 2 summarizes the post hoc Bonferroni's comparisons between paired age groups for these cardiac morphological and functional parameters.

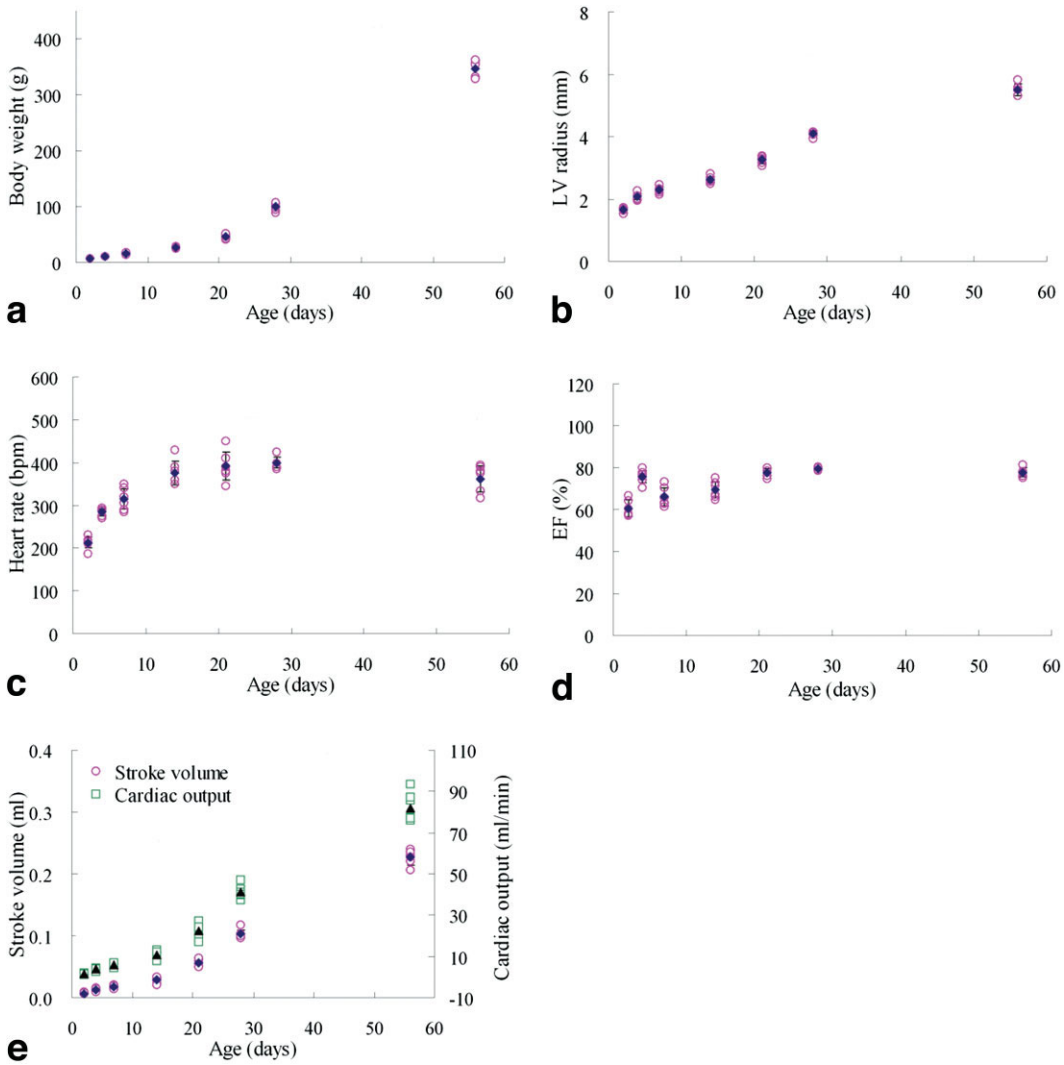

Figure 2. Changes of body weight (**a**), LV radius (**b**), heart rate (**c**), ejection fraction (EF, **d**), stroke volume (SV, e), and cardiac output (CO) with age. One-way ANOVA tests among all age groups were $P < 0.0001$ for all (a) to (e). [Color figure can be viewed in the online issue, which is available at www.interscience.wiley.com.]

Table 1
Correlations of the Parameters of Cardiac Morphology and Function

	Heart rate	Ejection fraction	Stroke volume	Cardiac output
Body weight	0.36	0.43	0.98	0.97
LV radius	0.64	0.63	0.97	0.98

Structurally, FA was found to increase significantly from day 2 (0.56 ± 0.01) to day 4 (0.61 ± 0.01), and gradually decreased up to day 56 (0.40 ± 0.02; Fig. 3a). Figure 3b–d illustrates the alterations of mean ADC, axial and radial diffusivities with age. From day 2 to day 4, significant increase of mean ADC (3.88 ± 0.17 to 5.70 ± 0.19 × 10^{-4} mm^2/s) was observed, resulting from the significant increase of the axial diffusivity (7.49 ± 0.30 to 10.42 ± 0.33 × 10^{-4} mm^2/s). Radial diffusivity increased gradually until day 7, while axial diffusivity decreased significantly from day 4 to day 56. The reversing development trends of these two directional diffusivities gave rise to the slight decrease of mean ADC. Table 3 summarizes the post hoc Bonferroni's comparisons between paired age groups for these DTI parameters.

The typical maps of FA, mean ADC, axial diffusivity, radial diffusivity, and helix angle at each postnatal time point are illustrated in Figures 4a–e, respectively. The helix angle maps revealed that a similar pattern was present among the samples from different age groups studied. Viewed from apex, myocardial fibers changed smoothly from the left-handed orientation in epicardium to the right-handed in endocardium. The transmural helix angle typically ranged from −60° at epicardium to +60° at endocardium. Such double-helical structure was apparent as early as day 2.

Figure 5 shows the H&E stain of the samples at each postnatal time point. A portion of mid-myocardium in middle short-axis slice (where fibers were circumferentially oriented) was selected for structural visualization (Fig. 5a). Figure 5b shows the myocardium structure at ×400 magnifications. Myocyte packing density was seen to decrease apparently at day 7 with increase of extracellular space.

DISCUSSION

During the postnatal period examined, body weight and LV radius increased substantially with age. Concurrently, SV and CO increased in response to the increasing hemodynamic load after birth (36). Heart rate gradually increased from ~200 to ~400 beats per minute (bpm) under isoflurane anesthesia from day 2 to day 28, but dropped to ~360 bpm at day 56. Ejection fraction increased within the first 4 days, decreased at day 7 and gradually increased until day 21. Note that such dramatic change in EF during early postnatal period was also observed in human infants between postnatal month 2 and 14 (37). In the current study, EF became stable after day 21, suggesting cardiac functional maturation at day 21. The cardiac functional maturation has been regarded as the maturation of structural organization and stable ratio of nonmyofibrillar elements to myofibrillar elements (3).

In the current study, myocardial fiber parameters (described by FA, mean ADC, axial and radial diffusivities) were assessed to monitor the alterations of diffusion anisotropy and diffusivities with age. From day 2 to

Table 2
Post Hoc Bonferroni's Multiple Comparison Tests Between Paired Age Groups for the Parameters of Cardiac Morphology and Function

Body weight	P2	P4	P7	P14	P21	P28
P4	ns					
P7	ns	ns				
P14	*	ns	ns			
P21	***	***	***	*		
P28	***	***	***	***	***	
P56	***	***	***	***	***	***

LV radius	P2	P4	P7	P14	P21	P28
P4	***					
P7	***	ns				
P14	***	***	***			
P21	***	***	***	***		
P28	***	***	***	***	***	
P56	***	***	***	***	***	***

Heart rate	P2	P4	P7	P14	P21	P28
P4	***					
P7	***	ns				
P14	***	***	**			
P21	***	***	***	ns		
P28	***	***	***	ns	ns	
P56	***	***	*	ns	ns	ns

EF	P2	P4	P7	P14	P21	P28
P4	***					
P7	ns	(***)				
P14	***	ns	ns			
P21	***	ns	***	**		
P28	***	ns	***	***	ns	
P56	***	ns	***	**	ns	ns

Stroke volume	P2	P4	P7	P14	P21	P28
P4	ns					
P7	ns	ns				
P14	***	**	ns			
P21	***	***	***	***		
P28	***	***	***	***	***	
P56	***	***	***	***	***	***

Cardiac output	P2	P4	P7	P14	P21	P28
P4	ns					
P7	ns	ns				
P14	***	*	ns			
P21	***	***	***	***		
P28	***	***	***	***	***	
P56	***	***	***	***	***	***

* $P < 0.05$; ** $P < 0.01$, *** $P < 0.001$, later age group significantly higher than earlier age group; (*)$P < 0.05$; (**)$P < 0.01$, (***)$P < 0.001$, later age group significantly lower than earlier age group; ns: not significant.

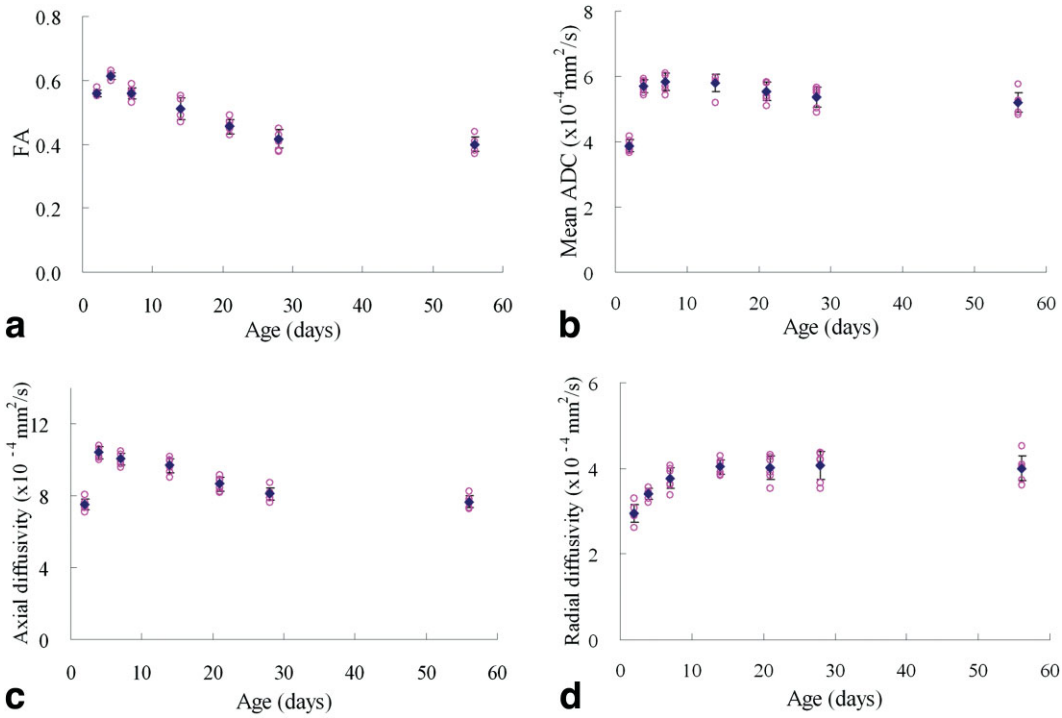

Figure 3. Changes of fractional anisotropy (FA, **a**), mean apparent diffusion coefficient (ADC, **b**), and axial (**c**), and radial (**d**) diffusivities with age. One-way ANOVA tests among all age groups were $P < 0.0001$ for all (a) to (d). [Color figure can be viewed in the online issue, which is available at www.interscience.wiley.com.]

day 4, significant increase of axial diffusivity was observed, resulting in mean ADC increase. Likely, these changes reflected the increase of intracellular and extracellular space (38,39) and the transition from hyperplasia to hypertrophy (13). From day 4 to day 56, axial diffusivity began to decrease while radial diffusivity gradually increased, suggesting the myocardial fiber hypertrophy occurring mainly along radial rather than axial directions. The alterations of these two directional diffusivities led to decrease of FA and mean ADC. From the H&E histology, myocyte density at day 2 and day 4 was higher than that at other time points, which corresponded to the myocyte hyperplasia stage as characterized using histological methods (10–13). From day 4 to day 7, extracellular space was observed to increase apparently, which might provide space for the following myocyte hypertrophy and contribute to the radial diffusivity increase and FA decrease observed. After day 7, myocardial fiber width was apparently larger than those at day 2 and day 4, reflecting the myocyte hypertrophy (10–13) and likely leading to the slight but continuous increase of radial diffusivity. After day 21, no significant alteration of myocardial fiber structure was observed, indicating the structural maturation by this

Table 3
Post Hoc Bonferroni's Multiple Comparison Tests Between Paired Age Groups for the Ex Vivo DTI Parameters of the Cardiac Structure

FA	P2	P4	P7	P14	P21	P28
P4	**					
P7	ns	(**)				
P14	(*)	(***)	(*)			
P21	(***)	(***)	(***)	(**)		
P28	(***)	(***)	(***)	(***)	ns	
P56	(***)	(***)	(***)	(***)	(**)	ns

Mean ADC	P2	P4	P7	P14	P21	P28
P4	***					
P7	***	ns				
P14	***	ns	ns			
P21	***	ns	ns	ns		
P28	***	ns	ns	ns	ns	
P56	***	ns	(*)	(*)	ns	ns

Axial diffusivity	P2	P4	P7	P14	P21	P28
P4	***					
P7	***	ns				
P14	***	(*)	ns			
P21	***	(***)	(***)	(***)		
P28	ns	(***)	(***)	(***)	ns	
P56	ns	(***)	(***)	(***)	(**)	ns

Radial diffusivity	P2	P4	P7	P14	P21	P28
P4	ns					
P7	***	ns				
P14	***	**	ns			
P21	***	**	ns	ns		
P28	***	**	ns	ns	ns	
P56	***	*	ns	ns	ns	ns

*$P < 0.05$; **$P < 0.01$, ***$P < 0.001$, later age group significantly higher than earlier age group; (*)$P < 0.05$; (**)$P < 0.01$, (***)$P < 0.001$, later age group significantly lower than earlier age group; ns: not significant.

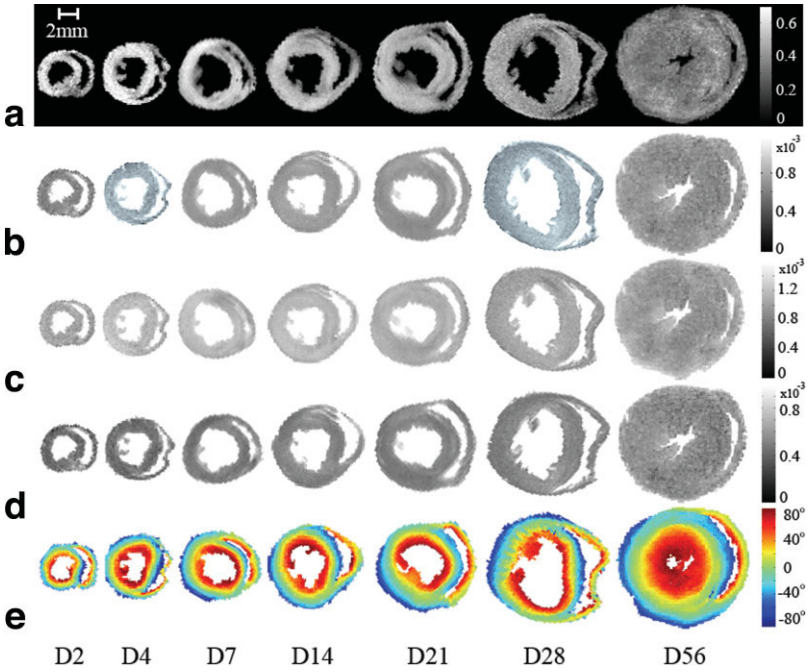

Figure 4. Fractional anisotropy (FA, **a:**), mean apparent diffusion coefficient (ADC, **b**), axial diffusivity (**c**), radial diffusivity (**d**), and helix angle maps (**e**) of myocardial fiber at different ages. Double-helical structure was apparent at as early as postnatal day 2. Note that each type of map is displayed with the same scale for all time points. [Color figure can be viewed in the online issue, which is available at www.interscience.wiley.com.]

time point. Furthermore, the current study also confirmed the presence of basic double-helical structure of myocardial fibers at a very early stage. This architecture was observed to start to form during embryonic ventricular growth (40). This unique structure has proved to be essential for dispersing strain uniformly and conserving energy expenditure (41). Note that whether and how such basic double-helical structure changes during early postnatal development remains to be investigated in the future, possibly with high-resolution DTI and arresting all heart samples precisely as the same cardiac points.

Several limitations existed in the current study. First, the rate of heart growth could be affected by litter size due to different preweanling nutritional state. Smaller litter size has been previously reported to cause accelerated heart growth associated with increased proliferation of cardiac muscle cells during postnatal heart development (42,43). In the current study, similar litter size was maintained (~8 rats /litter) before the rats were weaned at 21 days of age to minimize the influence. Second, water diffusion properties were found to alter with temperature and fixative solutions due to the compartmental nature of tissues and alteration in membrane permeability (44). In the current study, all samples were fixed with the same solution and kept in the similar temperature (~20°C) during the experiment. Third, it is noteworthy that formalin fixation can alter the diffusion environments, leading to different quantification from in vivo situation. However, the qualitative characteristics of the myocardial fiber structure assessed by DTI of formalin fixed heart are likely to remain true for intact myocardium. Lastly, the use of isoflurane during in vivo CMR study may affect cardiac function and result in lower EF and higher SV than those obtained in conscious rats (45). However, the trend of cardiac functional maturation may likely remain true.

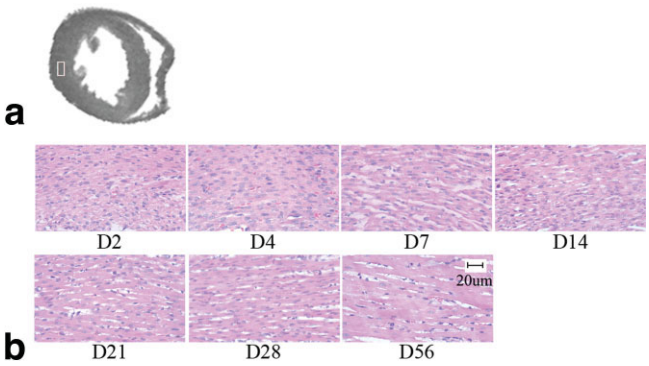

Figure 5. H&E histology was performed in heart samples of different age. A rectangular portion of the mid myocardium with circumferentially orientated fibers was selected (**a:**, white rectangular box), and myocardium structure was visualized at ×400 magnifications (**b**). [Color figure can be viewed in the online issue, which is available at www.interscience.wiley.com.]

In conclusion, postnatal development of cardiac function and myocardium structure was documented using in vivo CMR and ex vivo DTI in rats for the first time. Body weight and LV radius increased with age. Concurrently, stroke volume and cardiac output increase with age/body weight. The heart rate and ejection fraction was observed to stabilize after postnatal day 14 and 21, respectively. Fractional anisotropy, mean ADC and axial diffusivity increased within the first 4 days. Then radial diffusivity increased until day 7 while the other parameters decreased up to day 56. Double-helical myocardial fiber structure was found to be present as early as day 2. These experimental results can serve as the essential baselines for analysis of postnatal heart development. They also demonstrate the ability of DTI in detecting myocardium microstructural

changes at cellular level. As in vivo heart DTI is becoming feasible in humans (30), DTI characterization may lead to new clinical means to assess and monitor the myocardial structure and function in developmental or congenital heart diseases.

ACKNOWLEDGMENTS

The authors thank Mr. Kevin C. Chan and Dr. Kexia Cai at Laboratory of Biomedical Imaging and Signal Processing at The University of Hong Kong for technical assistance.

REFERENCES

1. Zak R, Kizu A, Bugaisky L. Cardiac hypertrophy: its characteristics as a growth process. Am J Cardiol 1979;44:941–946.
2. Novak F, Tvrzicka E, Hamplova B, Kolar F, Novakova O. Postnatal development of phospholipids and their fatty acid profile in rat heart. Mol Cell Biochem 2006;293:23–33.
3. Hopkins SF Jr, McCutcheon EP, Wekstein DR. Postnatal changes in rat ventricular function. Circ Res 1973;32:685–691.
4. Lee JC, Taylor FN, Downing SE. A comparison of ventricular weights and geometry in newborn, young, and adult mammals. J Appl Physiol 1975;38:147–150.
5. Hew KW, Keller KA. Postnatal anatomical and functional development of the heart: a species comparison. Birth Defects Res B Dev Reprod Toxicol 2003;68:309–320.
6. Wekstein DR. Heart rate of the preweanling rat and its autonomic control. Am J Physiol 1965;208:1259–1262.
7. Dowell RT. Metabolic and contractile function enhancement during rat heart postnatal development. Mech Ageing Dev 1984;25:307–321.
8. Rakusan K, Cicutti N, Flanagan MF. Changes in the microvascular network during cardiac growth, development, and aging. Cell Mol Biol Res 1994;40:117–122.
9. Gray SD. Pressure profiles in neonatal spontaneously hypertensive rats. Biol Neonate 1984;45:25–32.
10. Bugaisky L, Zak R. Cellular growth of cardiac muscle after birth. Tex Rep Biol Med 1979;39:123–138.
11. Perloff JK. Development and regression of increased ventricular mass. Am J Cardiol 1982;50:605–611.
12. Anversa P, Ricci R, Olivetti G. Quantitative structural analysis of the myocardium during physiologic growth and induced cardiac hypertrophy: a review. J Am Coll Cardiol 1986;7:1140–1149.
13. Li F, Wang X, Capasso JM, Gerdes AM. Rapid transition of cardiac myocytes from hyperplasia to hypertrophy during postnatal development. J Mol Cell Cardiol 1996;28:1737–1746.
14. Oparil S, Bishop SP, Clubb FJ Jr. Myocardial cell hypertrophy or hyperplasia. Hypertension 1984;6:III38–III43.
15. Leu M, Ehler E, Perriard JC. Characterisation of postnatal growth of the murine heart. Anat Embryol (Berl) 2001;204:217–224.
16. Arts T, Reneman RS, Veenstra PC. A model of the mechanics of the left ventricle. Ann Biomed Eng 1979;7:299–318.
17. Rademakers FE, Rogers WJ, Guier WH, et al. Relation of regional cross-fiber shortening to wall thickening in the intact heart. Three-dimensional strain analysis by NMR tagging. Circulation 1994;89: 1174–1182.
18. Taber LA, Yang M, Podszus WW. Mechanics of ventricular torsion. J Biomech 1996;29:745–752.
19. Smiseth OA, Remme EW. Regional left ventricular electric and mechanical activation and relaxation. J Am Coll Cardiol 2006;47: 173–174.
20. Geerts L, Bovendeerd P, Nicolay K, Arts T. Characterization of the normal cardiac myofiber field in goat measured with MR-diffusion tensor imaging. Am J Physiol Heart Circ Physiol 2002;283:H139–H145.
21. Scollan DF, Holmes A, Winslow R, Forder J. Histological validation of myocardial microstructure obtained from diffusion tensor magnetic resonance imaging. Am J Physiol 1998;275:H2308–2318.
22. Wu EX, Wu Y, Tang H, et al. Study of myocardial fiber pathway using magnetic resonance diffusion tensor imaging. Magn Reson Imaging 2007;25:1048–1057.
23. Chen J, Liu W, Zhang H, et al. Regional ventricular wall thickening reflects changes in cardiac fiber and sheet structure during contraction: quantification with diffusion tensor MRI. Am J Physiol Heart Circ Physiol 2005;289:H1898–H1907.
24. Helm PA, Tseng HJ, Younes L, McVeigh ER, Winslow RL. Ex vivo 3D diffusion tensor imaging and quantification of cardiac laminar structure. Magn Reson Med 2005;54:850–859.
25. Jiang Y, Pandya K, Smithies O, Hsu EW. Three-dimensional diffusion tensor microscopy of fixed mouse hearts. Magn Reson Med 2004;52:453–460.
26. Heemskerk AM, Strijkers GJ, Vilanova A, Drost MR, Nicolay K. Determination of mouse skeletal muscle architecture using three-dimensional diffusion tensor imaging. Magn Reson Med 2005;53: 1333–1340.
27. Holmes AA, Scollan DF, Winslow RL. Direct histological validation of diffusion tensor MRI in formaldehyde-fixed myocardium. Magn Reson Med 2000;44:157–161.
28. Hsu EW, Muzikant AL, Matulevicius SA, Penland RC, Henriquez CS. Magnetic resonance myocardial fiber-orientation mapping with direct histological correlation. Am J Physiol 1998;274:H1627–H1634.
29. Chen J, Song SK, Liu W, et al. Remodeling of cardiac fiber structure after infarction in rats quantified with diffusion tensor MRI. Am J Physiol Heart Circ Physiol 2003;285:H946–H954.
30. Wu MT, Tseng WY, Su MY, et al. Diffusion tensor magnetic resonance imaging mapping the fiber architecture remodeling in human myocardium after infarction: correlation with viability and wall motion. Circulation 2006;114:1036–1045.
31. Wu EX, Wu Y, Nicholls JM, et al. MR diffusion tensor imaging study of postinfarct myocardium structural remodeling in a porcine model. Magn Reson Med 2007;58:687–695.
32. Wu Y, Chan CW, Nicholls JM, Liao S, Tse HF, Wu EX. MR study of the effect of infarct size and location on left ventricular functional and microstructural alterations in porcine models. J Magn Reson Imaging 2009;29:305–312.
33. Strijkers GJ, Bouts A, Blankesteijn WM, et al. Diffusion tensor imaging of left ventricular remodeling in response to myocardial infarction in the mouse. NMR Biomed 2009;22:182–190.
34. Chaudhry HW, Dashoush NH, Tang H, et al. Cyclin A2 mediates cardiomyocyte mitosis in the postmitotic myocardium. J Biol Chem 2004;279:35858–35866.
35. Jiang H, van Zijl PC, Kim J, Pearlson GD, Mori S. DtiStudio: resource program for diffusion tensor computation and fiber bundle tracking. Comput Methods Programs Biomed 2006;81:106–116.
36. Claycomb WC. Cardiac-muscle hypertrophy. Differentiation and growth of the heart cell during development. Biochem J 1977;168: 599–601.
37. Oberhansli I, Brandon G, Friedli B. Echocardiographic growth patterns of intracardiac dimensions and determination of function indices during the first year of life. Helv Paediatr Acta 1981;36:325–340.
38. Olivetti G, Anversa P, Loud AV. Morphometric study of early postnatal development in the left and right ventricular myocardium of the rat. II. Tissue composition, capillary growth, and sarcoplasmic alterations. Circ Res 1980;46:503–512.
39. Jiang Y, Guccione JM, Ratcliffe MB, Hsu EW. Transmural heterogeneity of diffusion anisotropy in the sheep myocardium characterized by MR diffusion tensor imaging. American journal of physiology 2007;293:H2377–H2384.
40. Tobita K, Garrison JB, Liu LJ, Tinney JP, Keller BB. Three-dimensional myofiber architecture of the embryonic left ventricle during normal development and altered mechanical loads. Anat Rec A Discov Mol Cell Evol Biol 2005;283:193–201.
41. Vendelin M, Bovendeerd PH, Engelbrecht J, Arts T. Optimizing ventricular fibers: uniform strain or stress, but not ATP consumption, leads to high efficiency. Am J Physiol Heart Circ Physiol 2002;283:H1072–H1081.
42. Hollenberg M, Honbo N, Samorodin AJ. Cardiac cellular responses to altered nutrition in the neonatal rat. Am J Physiol 1977;233: H356–H360.
43. Rakusan K, Raman S, Layberry R, Korecky B. The influence of aging and growth on the postnatal development of cardiac muscle in rats. Circ Res 1978;42:212–218.
44. Thelwall PE, Shepherd TM, Stanisz GJ, Blackband SJ. Effects of temperature and aldehyde fixation on tissue water diffusion properties, studied in an erythrocyte ghost tissue model. Magn Reson Med 2006;56:282–289.
45. Stein AB, Tiwari S, Thomas P, et al. Effects of anesthesia on echocardiographic assessment of left ventricular structure and function in rats. Basic Res Cardiol 2007;102:28–41.